Reaction of Hydrogen Atoms with Propyne at High Temperatures: An Experimental and Theoretical Study †

ARTICLE *in* THE JOURNAL OF PHYSICAL CHEMISTRY A · JUNE 2007

Impact Factor: 2.69 · DOI: 10.1021/jp070833c · Source: PubMed

6 AUTHORS, INCLUDING:

Binod R Giri
King Abdullah University of Science and Tech…
27 PUBLICATIONS **208** CITATIONS
SEE PROFILE

Milán Szőri
University of Szeged
41 PUBLICATIONS **338** CITATIONS
SEE PROFILE

Reaction of Hydrogen Atoms with Propyne at High Temperatures: An Experimental and Theoretical Study†

Tobias Bentz, Binod R. Giri,‡ Horst Hippler, Matthias Olzmann,* Frank Striebel,§ and Milan Szöri||

Institut für Physikalische Chemie, Universität Karlsruhe (TH), Kaiserstr. 12, 76128 Karlsruhe, Germany

Received: January 31, 2007; In Final Form: February 19, 2007

The kinetics of the reaction of hydrogen atoms with propyne (pC_3H_4) was experimentally studied in a shock tube at temperatures ranging from 1200 to 1400 K and pressures between 1.3 and 4.0 bar with Ar as the bath gas. The hydrogen atoms (initial mole fraction 0.5−2.0 ppm) were produced by pyrolysis of C_2H_5I and monitored by atomic resonance absorption spectrometry under pseudo-first-order conditions with respect to propyne (initial mole fraction 5−20 ppm). From the hydrogen atom time profiles, overall rate coefficients $k_{ov} \equiv -([pC_3H_4][H])^{-1} \times d[H]/dt$ for the reaction $H + pC_3H_4 \rightarrow$ products ($\neq H$) were deduced; the following temperature dependence was obtained: $k_{ov} = 1.2 \times 10^{-10} \exp(-2270\ K/T)\ cm^3\ s^{-1}$ with an estimated uncertainty of ±20%. A pressure dependence was not observed. The results are analyzed in terms of statistical rate theory with molecular and transition state data from quantum chemical calculations. Geometries were optimized using density functional theory at the B3LYP/6−31G(d) level, and single-point energies were computed at the QCISD(T)/cc-pVTZ level of theory. It is confirmed that the reaction proceeds via an addition−elimination mechanism to yield $C_2H_2 + CH_3$ and via a parallel direct abstraction to give $C_3H_3 + H_2$. Furthermore, it is shown that a hydrogen atom catalyzed isomerization channel to allene (aC_3H_4), $H + pC_3H_4 \rightarrow aC_3H_4 + H$, is also important. Kinetic parameters to describe the channel branching of these reactions are deduced.

1. Introduction

The formation of aromatic hydrocarbons from aliphatic precursors under combustion conditions has become an important topic of research. Two major reaction routes to the first aromatic ring are discussed, one involving C_2 and one involving C_3 building units.[1−6] In this context, the multichannel reaction of propyne with hydrogen atoms

$$CH_3CCH + H \rightarrow \text{products} \qquad (1)$$

is important, because it can interconnect these two reaction routes via the channel

$$CH_3CCH + H \leftrightarrow C_2H_2 + CH_3 \qquad (2,–2)$$

which actually consists of two consecutive steps:

$$CH_3CCH + H \leftrightarrow CH_3CHCH \qquad (2a,–2a)$$

and

$$CH_3CHCH \leftrightarrow C_2H_2 + CH_3 \qquad (2b,–2b)$$

Reaction 1 can furthermore provide a source for propargyl radicals via the direct abstraction channel

$$CH_3CCH + H \leftrightarrow CH_2CCH + H_2 \qquad (3,–3)$$

and also catalyze the mutual isomerization of propyne and allene via

$$CH_3CCH + H \leftrightarrow CH_2CCH_2 + H \qquad (4,–4)$$

a reaction, which again proceeds in two consecutive steps:

$$CH_3CCH + H \leftrightarrow CH_3CCH_2 \qquad (4a,–4a)$$

and

$$CH_3CCH_2 \leftrightarrow CH_2CCH_2 + H \qquad (4b,–4b)$$

Wherever appropriate in the text, we will abbreviate propyne by pC_3H_4 and allene by aC_3H_4.

The first kinetic study of reaction 1, to our knowledge, was performed by Brown and Thrush.[7] These authors carried out experiments in a discharge-flow reactor at room temperature and at pressures between 1 and 3 mbar. Hydrogen atoms were detected by electron spin resonance (ESR), and an overall rate coefficient,

$$k_{ov} = -\frac{1}{[pC_3H_4][H]} \times \frac{d[H]}{dt} \qquad (5)$$

was determined; a value $k_{ov} = (4.0 \pm 0.5) \times 10^{-13}\ cm^3\ s^{-1}$ was obtained. A few years later, Wagner and Zellner[8] used a similar experimental setup to study the temperature dependence

† Part of the special issue "James A. Miller Festschrift".

* Corresponding author. E-mail: olzmann@chem-bio.uni-karlsruhe.de.

‡ Present address: Argonne National Laboratory, Chemistry Division Building 200, 9700 South Cass Avenue, Argonne, IL 60439-4831.

§ Present address: Abgaszentrum der Automobilindustrie ADA, c/o Dr. Ing. h.c. F. Porsche AG, Porschestr., 71287 Weissach, Germany.

|| Present address: Department of Chemistry and Chemical Informatics, Faculty of Education, University of Szeged, H-6701 Szeged, P. O. Box 396, Hungary.

10.1021/jp070833c CCC: $37.00
Published on Web 03/23/2007

of reaction 1. Besides the detection of hydrogen atoms by ESR, stable products were determined by gas chromatography and mass spectrometry. For the temperature dependence of the rate coefficients k_2 and k_{4a} at pressures between 1.3 and 24 mbar and temperatures between 195 and 503 K, the following Arrhenius expressions were obtained: $k_2 = (9.6 \pm 2.0) \times 10^{-12}$ exp[$-(13 \pm 1)$ kJ mol^{-1}/RT] cm^3 s^{-1} and $k_{4a} = (1.1 \pm 0.2) \times 10^{-11}$ exp[$-(8.8 \pm 0.9)$ kJ mol^{-1}/RT] cm^3 s^{-1}; that is, the terminal addition, eq 4a, is faster than reaction 2 induced by the non-terminal addition, eq 2a. In a further investigation of the temperature dependence ($T = 215-460$ K, $P = 7-800$ mbar), Whytock et al.[9] used flash photolysis for the production of hydrogen atoms in propyne/argon mixtures and time-resolved resonance fluorescence for their detection. High-pressure limiting values for k_{ov} were determined, and their temperature dependence was represented in the form $k_{ov}^{\infty} = (6.0 \pm 1.2) \times 10^{-11}$ exp[$-(10.3 \pm 0.4)$ kJ mol^{-1}/RT] cm^3 s^{-1}. In these experiments, the high-pressure limit is reached at pressures of about 400 mbar for $T = 460$ K and at pressures of ~100 mbar for $T = 300$ K.

Despite its importance in hydrocarbon combustion and pyrolysis, there are only very few kinetic studies of reaction 1 at temperatures above 1000 K. The rate data in this temperature range were either computed from statistical rate theory or deduced from pyrolysis experiments by complex modeling. In a shock-tube study of propyne and allene decomposition ($T = 1200-1570$ K, $P = 1.7-2.6$ bar), Hidaka et al.[10] were able to fit their results in terms of a 34-step mechanism with a rate coefficient $k_2 = 2.2 \times 10^{-19}$ (T/K)$^{2.5}$ exp[-4.2 kJ mol^{-1}/RT] cm^3 s^{-1}, which gives absolute values of k_2 in reasonable agreement with the results of ref 8 mentioned above and an early estimation of Warnatz et al.[11] adopted by Wu and Kern.[12] From C_3H_4 profiles in a premixed ethane−oxygene flame, Ancia et al.[13] deduced a rate coefficient of 7.5×10^{-12} cm^3 s^{-1} for the $C_3H_4 + H$ reaction at 1660 K and pressures between 20 and 100 mbar. Since mass-spectrometric detection was used, the authors were not able to distinguish between propyne and allene.

Apart from a global assessment,[14] a first theoretical study of parts of the underlying C_3H_5 potential energy surface was performed by Diau et al.[15] These authors calculated rate coefficients for the competing steps of the $C_2H_2 + CH_3$ reaction with the Rice−Ramsperger−Kassel−Marcus (RRKM) theory based on molecular and transition state data predicted by the BAC-MP4 method. Kinetic parameters for reaction 1, however, were not deduced. More recently, in a combined experimental and theoretical study, Davis et al.[16] computed temperature- and pressure-dependent rate coefficients for reactions on the C_3H_5 potential energy surface (including reaction sequences 2 and 4) using the RRKM theory. In their work, the molecular and transition state data were obtained from the density functional theory (DFT, B3−PW91/6-311G(d,p)), and the energy barriers were obtained from calculations at the G2//B3LYP/6-31G(d) level. The results were employed to simulate concentration−time profiles from propyne pyrolysis experiments in a flow reactor. Another detailed theoretical analysis of reaction 1 was performed by Wang et al.[17] In this work, multichannel RRKM and transition state calculations were performed on the basis of results from quantum chemical computations at the G3//B3LYP/6-31G(d) level of theory. The kinetic data of the last two studies[16,17] are complex and will be discussed together with our own results in section 4.

Since all of the experimental kinetic data for reaction 1 at temperatures above 500 K have been obtained from fitting to complex mechanisms, we performed a shock-tube study of reaction 1 with a direct time-resolved detection of hydrogen atoms. The H atoms were formed in an excess of propyne by the fast thermal decomposition of C_2H_5I via the reaction sequence

$$C_2H_5I \rightarrow C_2H_5 + I \quad (6)$$

$$C_2H_5 \rightarrow C_2H_4 + H \quad (7)$$

and detected by atomic resonance absorption spectrometry (ARAS).

The data are analyzed in terms of a small reaction mechanism consisting of 4 elementary steps with rate coefficients from the RRKM and transition state theory. To get a consistent set of molecular and transition state data, we performed quantum chemical calculations at the B3LYP/6-31G(d) level (geometries and harmonic frequencies) and at the QCISD(T)/cc-pVTZ level of theory (single-point energies). Our results will be compared with the results from G2[16] and G3[17] calculations.

2. Experimental Section

The experiments were performed in a stainless steel shock tube behind reflected shock waves at temperatures between 1200 and 1400 K and pressures between 1.3 and 4.0 bar with Ar as the bath gas. Since the experimental setup was described previously,[18,19] we will only give a brief summary here.

The high-pressure section of the shock tube is 3.05 m long with an inner diameter of 9.85 cm. It is separated by an aluminum foil from the low-pressure section, which is 4.20 m long and has an inner diameter of 10 cm. The shock waves were initiated by pressure bursting of the aluminum foil, where different foils with thicknesses between 40 and 100 μm were used depending on the desired temperature and pressure. Hydrogen served as the driver gas, and the driven gas was argon containing a small fraction of propyne (5−20 ppm) and ethyl iodide (0.5−2.0 ppm). The concentration ratio between ethyl iodide and propyne was varied between 1:10 and 1:20. Because of the low concentrations of propyne and ethyl iodide, the test gas mixture could be treated as an ideal gas, and the post-shock conditions were calculated from the initial temperature, pressure, and the shock wave velocity by applying one-dimensional conservation equations (see, e.g., ref 20). The shock wave velocity was measured with four pressure transducers (Kistler, 603B), which were placed 40 cm apart from each other with the last one being located ~10 cm from the end plate of the shock tube.

The hydrogen atom concentration was monitored by ARAS at the Lyman α line (121.6 nm). The vacuum ultraviolet (VUV) radiation is produced in a microwave-discharge lamp consisting of a quartz tube with a mounted resonator. The resonator is connected to a microwave generator (Muegge), which operates at 2.45 GHz with a typical output power of 100 W. A mixture of ~1% H_2 in helium is flown through the quartz tube at a constant pressure of ~7 mbar. The VUV light is transmitted via MgF_2 windows through the shock tube to a VUV monochromator (Acton Research Corp., Spectra Pro VM-504) and detected with a solar-blind photomultiplier (Hamamatsu R1259). The signal from the photomultiplier is sampled by a digital storage oscilloscope (Tektronix TDS 540A) and further processed in a personal computer. Because of the poorly characterized emission profile of the microwave-discharge lamp, one cannot use the Beer−Lambert law to convert absorbances to concentrations. Instead, one has to do calibration experiments

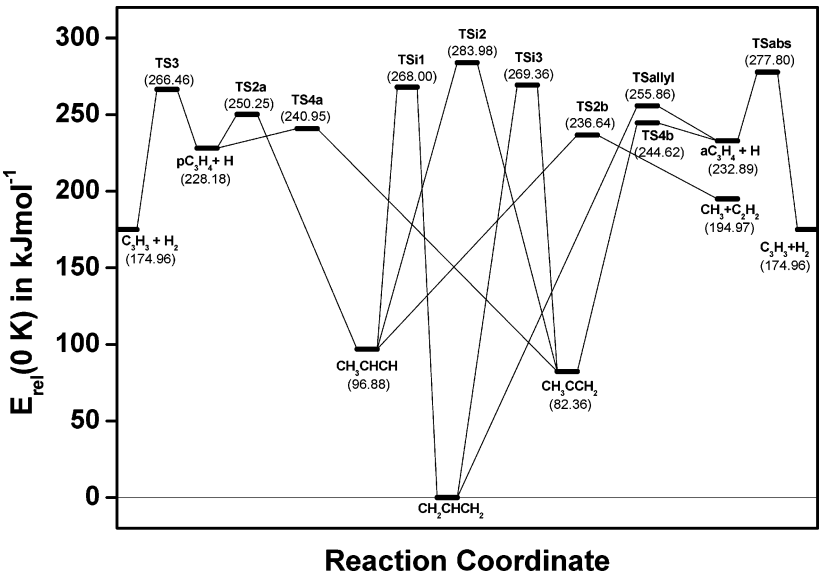

Figure 1. Potential energy diagram for the C_3H_5 reactions calculated at the QCISD(T)/cc-pVTZ//B3LYP/6-31G(d) level of theory (including zero-point energy).

with a well-characterized H atom source under similar conditions (T and P) as in the experiments. We have chosen a procedure based on N_2O/H_2 mixtures[21,22] and refer for details to a recent publication from our laboratory.[19] With the setup just described, we were able to quantitatively detect hydrogen atoms in concentrations between 3×10^{11} and 6×10^{13} cm^{-3}.

Prior to each experiment, the shock tube was evacuated to pressures below 5×10^{-6} mbar, and the cleanliness was regularly tested by performing shots with neat argon at temperatures above 2000 K. If H atoms were detected in these control experiments, cleaning was accomplished by carrying out shots with O_2 to remove possible contaminations from the shock-tube walls. This was repeated until no more background H atoms could be detected. The test gas and the calibration mixture were prepared in two different 100 dm^3 stainless steel mixing vessels, which were evacuated to pressures below 10^{-6} mbar before mixture preparation. Prior to use, the mixtures were allowed to homogenize for at least 20 h.

The purity of the gases and chemicals used were propyne (Aldrich) >98%, ethyl iodide (Fluka) >99.5% (propyne and ethyl iodide were degassed several times before using), H_2 for calibration (Messer Griesheim) >99.999%, H_2 as driver gas (Air Liquide) >99.8%, argon (Air Liquide) >99.9999%, and N_2O (Messer Griesheim) 99%.

3. Calculations

To analyze our experimental results in terms of statistical rate theory, we performed quantum chemical calculations for the stable species and the transition states on the C_3H_5 potential energy surface using the Gaussian 03 program package.[23] Rotational constants and harmonic frequencies were obtained from DFT[24] employing the Becke−3−Lee−Yang−Parr functional[25] with the Gaussian split valence basis set 6-31G(d).[26] For the optimized geometries, single-point energies were computed at the QCISD(T)/cc-pVTZ level of theory. Here, QCISD(T) stands for quadratic configuration interaction with single and double excitations including triples corrections,[27] and cc-pVTZ denotes Dunning's correlation consistent basis set.[28] The calculated potential energy profile is shown in Figure 1. Rotational constants and harmonic wavenumbers (scaled by a factor of 0.97)[29] are compiled in Table IS of Supporting Information. In the case of CH_3CHCH, the energetically more stable cis isomer was used in all of our kinetic calculations. The trans isomer was found to lie 2.0 kJ mol^{-1} higher in energy, and the energetic maximum between the two conformers lies 18.1 kJ mol^{-1} above the cis isomer (see also ref 17). The treatment of this cis−trans isomerization as a hindered rotation would probably slightly increase the density of states of CH_3CHCH but would not influence the branching between reaction 2a and reaction 2b, which is mainly determined by the properties of the respective transition states.

TABLE 1: Arrhenius Parameters for the High-Pressure Limiting Values of the Rate Coefficients Calculated from the Transition State Theory (T = 1000−1500 K)[a]

reaction	log A^∞	E_a^∞ (kJ mol^{-1})
2a	−9.28	33.3
−2a	14.63	167.3
2b	15.83	155.7
−2b	−9.54	59.1
3[b]	−9.25	52.3
4a	−8.46	25.7
−4a	15.32	174.0
4b	14.51	176.5
−4b	−8.93	24.1

[a] Units: cm^3, molecule, s. [b] Direct abstraction, pressure independent; $k_3 \equiv k_3^\infty$.

From the results of these quantum chemical calculations, rate coefficients for the direct bimolecular abstraction reaction, eq 3, and high-pressure limiting values of the rate coefficients for the complex-forming bimolecular steps, eqs 2a, 4a, −2b, and −4b and the unimolecular dissociation steps, eqs −2a, 2b, −4a, and 4b were calculated using the canonical transition state theory:[30,31]

$$k_i^\infty(T) = \frac{k_B T}{h} \frac{Q_{TSi}}{Q_{Ri}} \exp\left(-\frac{E_{0(i)}}{k_B T}\right) \quad (8)$$

Here, k_B is Boltzmann's constant, h is Planck's constant, and T is the temperature. The symbols Q_{TSi} and Q_{Ri} denote the partition functions of the transition state and the reactant(s), respectively, for the step i; $E_{0(i)}$ is the corresponding threshold energy. The results are compiled in Table 1.

The reaction sequence initiated by the $CH_3CCH + H$ reaction is in general a chemical activation system.[32−34] However, as is shown below, the thermal lifetimes of the intermediates CH_3CHCH and CH_3CCH_2 at our conditions are clearly below the

TABLE 2: Unimolecular Rate Coefficients $k_i(T,P)$ Calculated from Eqs 9−11

		CH_3CHCH			CH_3CCH_2		
T (K)	P (bar)	k_{-2a} (s^{-1})	k_{2b} (s^{-1})	k_{2b}/k_{-2a}	k_{-4a} (s^{-1})	k_{4b} (s^{-1})	k_{4b}/k_{-4a}
1200	1.3	5.44×10^3	1.38×10^6	254	4.50×10^5	4.51×10^4	0.100
	4.0	2.02×10^4	3.48×10^6	173	1.04×10^6	1.09×10^5	0.105
1300	1.3	8.68×10^3	2.20×10^6	253	8.32×10^5	8.36×10^4	0.100
	4.0	3.21×10^4	5.54×10^6	173	1.96×10^6	2.06×10^5	0.105
1400	1.3	1.22×10^4	3.10×10^6	253	1.32×10^6	1.32×10^5	0.100
	4.0	4.93×10^4	8.34×10^6	169	3.34×10^6	3.52×10^5	0.105

time scale of the experiment. Therefore, the chemical activation system is in its final steady state in the sense of ref 35, that is, the stabilization reservoir is filled up. Consequently, thermal rate coefficients $k_i(T,P)$ can be used in a good approximation for the characterization of the unimolecular decomposition steps of these intermediate radicals (see the early discussion of this topic in ref 35−37 and recent aspects reviewed in ref 38).

The thermal lifetimes, $\tau_i = [k_{-ia}(T,P) + k_{ib}(T,P)]^{-1}$ with $i = 2$ for CH_3CHCH and $i = 4$ for CH_3CCH_2, were computed from the lowest eigenvalue of the matrix **J** of the respective two-channel master equation,[32−34]

$$[\omega(\mathbf{I} - \mathbf{P}) + \mathbf{K_{-ia}} + \mathbf{K_{ib}}]\mathbf{N}^S \equiv \mathbf{J}\mathbf{N}^S = 0 \qquad (9)$$

Here, ω denotes the Lennard−Jones collision frequency, **I** is the unit matrix, **P** is the matrix of the collisional transition probabilities $P(E_k, E_j)$, and $\mathbf{K_{-ia}}$ and $\mathbf{K_{ib}}$ are diagonal matrices containing the specific rate coefficients $k_{-ia}(E_j)$ and $k_{ib}(E_j)$, respectively. The vector $\mathbf{N}^S$ represents the steady-state population $n^s(E_j; T,P)$ of the reacting intermediate at a given temperature and pressure. The specific rate coefficients were obtained from the RRKM theory:[32−34,39]

$$k_i(E) = \frac{W_{TSi}(E - E_{0(i)})}{h\rho_i(E)} \qquad (10)$$

where $W_{TSi}(E)$ denotes the sum of states of the transition state for reaction i and $\rho_i(E)$ is the density of states of the corresponding intermediate. The one-channel thermal rate coefficients then follow by averaging $k_i(E)$ over the steady-state distribution n^S:

$$k_i(T,P) = \int_0^\infty k_i(E) n^S(E;T,P)\, dE \qquad (11)$$

In our calculations, the isomerization reactions via the high-lying, tight transition states TS*i*1, TS*i*2, and TS*i*3 (see Figure 1) are neglected because they are much slower than the dissociation steps.[16,17]

For the transition probabilities, a stepladder model obeying detailed balancing was used.[32,33] The step size (corresponding to the average energy transferred per down collision) and the Lennard−Jones parameters were adopted from our study of the allyl radical decomposition:[19] $\Delta E_{SL} = 320\ cm^{-1}$, $\sigma(Ar) = 3.47$ Å, $\epsilon(Ar) = 114$ K, $\sigma(C_3H_5) = 4.85$ Å, and $\epsilon(C_3H_5) = 260$ K. All densities and sums of states were determined by direct counting procedures[40−42] in the rigid rotor/harmonic oscillator approximation for a total angular momentum quantum number $J = 50$, which is the average J for the intermediate radicals at $T = 1300$ K. We adopted this value also for all other temperatures, because the influence of varying J is small because of the tight transition states in our system.[32,33] Equation 9 is set up with a bin size of 10 cm^{-1}. The lowest eigenvalue and the associated eigenvector were determined by standard routines for tridiagonal matrices.[43] Energy zero is the rovibrational ground state of the corresponding radical. More technical details of our master equation can be found in ref 44. Temperature- and pressure-dependent unimolecular rate coefficients and branching ratios calculated in this way are collected in Table 2.

4. Results and Discussion

Experiment. A typical concentration time profile of the hydrogen atoms under pseudo-first-order conditions with respect to propyne is shown in Figure 2. There is a fast increase caused by the decomposition of ethyl iodide followed by the decrease due to reaction 1. The signal does not decay exactly to zero, which is caused by background absorption probably from propyne. This is demonstrated by the red profile in Figure 2, which shows the absorption in an experiment under identical conditions but without ethyl iodide in the mixture. We note that in the temperature range of our investigation, no detectable amounts of hydrogen atoms from propyne decomposition are formed on the time scale of our experiment. A modeling has shown that only at the highest temperatures, above 1400 K, H atom concentrations near the detection limit occur at reaction times clearly above 1 ms.

The rate coefficients k_{ov} were obtained from first-order plots after the subtraction of the background absorption. By varying the propyne concentration, the pseudo-first-order condition and the absence of interfering bimolecular side reactions were confirmed. The rate coefficients obtained in this way are displayed in Figure 3 and compiled with the detailed reaction conditions in Table IIS of Supporting Information. A weak positive temperature dependence was found, which can be expressed in the form

$$k_{ov} = 1.2 \times 10^{-10} \exp(-2270\ K/T)\ cm^3\ s^{-1} \qquad (12)$$

No discernible pressure dependence was observed within our experimental uncertainty, and the maximum error for k_{ov} was estimated to be ±20%.

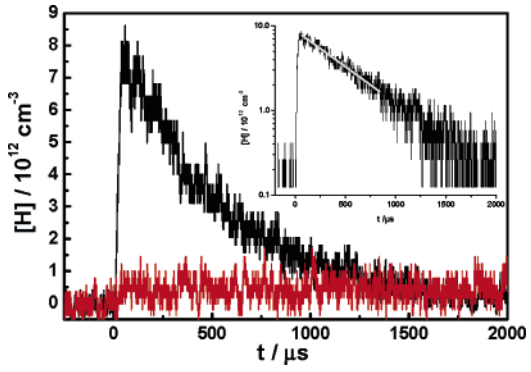

Figure 2. Concentration time profile (black line) at $T = 1230$ K, $P = 1360$ mbar, $[pC_3H_4]_0 = 9.6 \times 10^{13}\ cm^{-3}$, and $[C_2H_5I]_0 = 8.7 \times 10^{12}\ cm^{-3}$; background absorption from propyne (red line) formally expressed in terms of an equivalent H concentration (see text); pseudo-first-order plot and linear fit (inset).

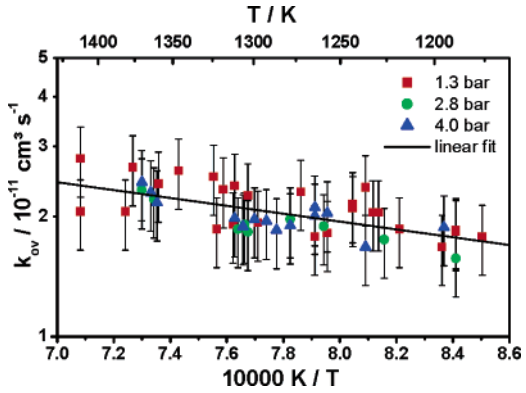

Figure 3. Temperature dependence of the experimental overall rate coefficients and linear fit resulting in eq 12.

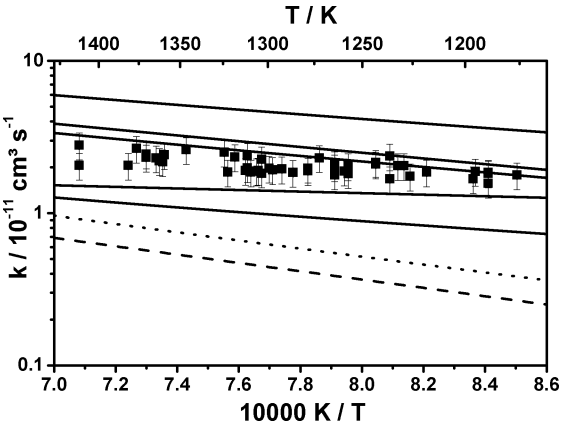

Figure 4. Comparison of the rate coefficients. Squares, k_{ov} from our experiments; lines, calculated or estimated values; solid lines (top to bottom), k_{tot} ($\sim k_2 + k_3$) from ref 17, $k_2 + k_3$ from this work, $k_2 + k_3$ from ref 16, $k_2 + k_3$ from ref 12, $k_2 + k_3$ from ref 10; dotted line, k_3 from ref 17; dashed line, k_3 from this work.

Calculations. The results of our quantum chemical computations performed at the QCISD(T)/cc-pVTZ// B3LYP/6-31G(d) level of theory are in very close accord with the results of the other two quantum chemical studies published (G2//B3LYP/6-31G(d)[16] and G3//B3LYP/6-31G(d)[17]). The differences of the relative energies do not exceed 6 kJ mol^{-1} and are often much less. A comparison with the very few experimental values available was made in ref 17 and is not repeated here; it also shows a very good agreement.

Data Analysis. As already mentioned, the experimentally obtained rate coefficient k_{ov} could not be assigned to one specific reaction channel, because there is no information in the observed hydrogen atom profile about the channel branching. Therefore, we will rely on our theoretical results for the discussion of the reaction mechanism. As already mentioned above, we will neglect isomerization reactions via the high-lying, tight transition states TS*i*1, TS*i*2, and TS*i*3.

We first note that the direct abstraction reaction, eq 3, has a barrier, which is ~16 kJ mol^{-1} higher than the barrier of reaction 2a and ~26 kJ mol^{-1} higher than the barrier of reaction 4a. The intermediate CH_3CHCH formed in reaction 2a either can react back to pC_3H_4 + H or further decompose via transition state 2b forming CH_3 and C_2H_2. The transition state 2b is located ~14 kJ mol^{-1} below TS2a. The thermal lifetime of the CH_3-$CHCH$ radical is, for example, at 1300 K and 1.3 bar, $\tau_2 = [k_{-2a} + k_{2b}]^{-1} \sim 5 \times 10^{-7}$ s and stays well below the time scale of our experiments over the temperature and pressure range considered in this work (cf. Table 2). Inspection of Table 2 also shows that the branching ratio k_{2b}/k_{-2a} is virtually independent of the temperature and only moderately pressure-dependent. In each case, the forward reaction, eq 2b, toward $CH_3 + C_2H_2$ is strongly favored.

Reaction 4a has the lowest energy barrier and is the fastest among all three pC_3H_4 + H channels. The intermediate CH_3-CCH_2 radical formed has a thermal lifetime of $\tau_4 = [k_{-4a} + k_{4b}]^{-1} \sim 1 \times 10^{-6}$ s at 1300 K and 1.3 bar. The branching ratio k_{4b}/k_{-4a} is about 0.1, virtually independent of temperature and pressure in the parameter range of this work (cf. Table 2); that is, back dissociation is favored here. As the overall reaction 4 conserves the number of hydrogen atoms, its rate coefficient is not accessible in our experiments.

In view of the high excess of propyne in our experiments, it is reasonable to neglect the allene (aC_3H_4) + H reactions, because at any time $[pC_3H_4] \gg [aC_3H_4]$. Neglecting, furthermore, the $CH_3 + C_2H_2$ reaction (comparatively high threshold energy) and assuming steady-state conditions for $[CH_3CHCH]$ and $[CH_3CCH_2]$, one obtains the following approximate rate laws:

$$\frac{d[H]}{dt} = -\left\{k_3 + k_{2a}^{\infty}\frac{k_{2b}}{k_{2b} + k_{-2a}}\right\}[pC_3H_4][H] \qquad (13)$$

$$\frac{d[C_2H_2]}{dt} = k_{2a}^{\infty}\frac{k_{2b}}{k_{2b} + k_{-2a}}[pC_3H_4][H] \qquad (14)$$

$$\frac{d[aC_3H_4]}{dt} = k_{4a}^{\infty}\frac{k_{4b}}{k_{4b} + k_{-4a}}[pC_3H_4][H] \qquad (15)$$

From eqs 5 and 13, it follows

$$k_{ov} = k_3 + k_{2a}^{\infty}\frac{k_{2b}}{k_{2b} + k_{-2a}} \qquad (16)$$

and, because $k_{2b} \gg k_{-2a}$ (see Table 2), $k_{ov} \sim k_3 + k_{2a}^{\infty}$. That is, reactions 2 and 3 almost exclusively govern the hydrogen atom time profile, and back dissociation of CH_3CHCH to pC_3H_4 + H, eq −2a, can be neglected (<1%). This is in line with other works.[15,17,45]

A comparison of our experimental results for k_{ov} with the calculated rate coefficients and earlier recommendations is made in Figure 4. The general agreement is satisfactory. The branching ratio k_2/k_3 from our calculations decreases from ~6 at 1200 K to ~3 at 1400 K. Similar ratios (~8 at 1200 K and ~6 at 1400 K) were obtained in the calculations of Wang et al.[17] though their absolute rate coefficients are slightly higher than our values. The results of the computations from ref 16 are in very good agreement with our calculations. We note that here the agreement in k_2 is nearly perfect (deviation <5 %) and that the difference to be seen in Figure 4 (second and third line from top) is mainly due to slightly different results for k_3. The evaluation from Hidaka et al.[10] and the Arrhenius expressions used in ref 12 give values somewhat below our experimental results. Furthermore, the data from ref 12 exhibit a too weak temperature dependence. This is mainly due to the temperature dependence of k_2, which was adopted from an early work of Warnatz et al.[11] These authors probably extrapolated low-temperature values for k_1 (the only values available at that time) to temperatures above 1000 K. The low-temperature values, however, are governed by the terminal addition, eq 4a, which has a lower activation energy than the non-terminal addition, eq 2a, prevailing at higher temperatures. Nonetheless, the absolute magnitude of the rate coefficients is in good agreement with the more recent calculated data and our experimental

TABLE 3: Kinetic Data for the Model Used in Our Simulation (T = 1200−1400 K, P = 1−4 Bar)[a]

eq	reaction	log A	E_a (kJ mol^{-1})	ref
6 + 7	$C_2H_5I \rightarrow C_2H_4 + I + H$	10.3[b]	132.2	47
2	$pC_3H_4 + H \rightarrow C_2H_2 + CH_3$	−9.28	33.3	this work
3	$pC_3H_4 + H \rightarrow C_3H_3 + H_2$	−9.25	52.3	this work
4	$pC_3H_4 + H \rightarrow aC_3H_4 + H$	−9.50	25.7	this work

[a] Units: cm^3, molecule, s. [b] Increased by 0.5, see text.

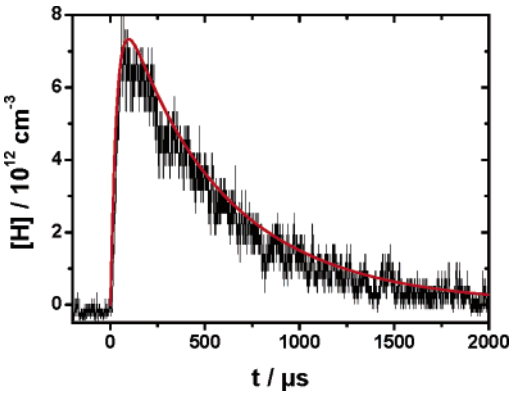

Figure 5. Measured (black line) and simulated (red curve) concentration−time profile (T = 1190 K, P = 1330 mbar, $[pC_3H_4]_0 = 9.8 \times 10^{13}$ cm^{-3}, $[C_2H_5I]_0 = 8.8 \times 10^{12}$ cm^{-3}); the signal lies below zero for $t < 0$ since pC_3H_4 background was subtracted (see discussion at the beginning of section 4 and Figure 2).

results. We also note that there is an inconsistency in the A factor of reaction 3 between ref 12 and the cited reference from Kiefer et al.[46] In Introduction, we mentioned that Ancia et al.[13] deduced a value $k(C_3H_4 + H \rightarrow \text{products}) \sim 7.5 \times 10^{-12}$ cm^3 s^{-1} for T = 1660 K and pressures below 100 mbar from flame profiles. Compared to our transition state calculations, which give for these conditions $k_2 + k_3 \sim (5.0 + 1.4) \times 10^{-11}$ cm^3 s^{-1}, this value appears too low.

An interesting mechanistic implication is revealed by a numerical comparison of eqs 14 and 15. From the values contained in Tables 1 and 2, one obtains $k_4 = k_{4a}^{\infty} \times k_{4b}/(k_{4b} + k_{-4a}) \sim k_{4a}^{\infty} \times 0.09$ (independent of temperature and pressure), which means that k_4 and $k_2 \sim k_{2a}^{\infty}$ are in the same order of magnitude. The higher relative fraction of back dissociation (∼90%) in the reaction sequence 4a,−4b is compensated by the higher capture rate coefficient, k_{4a}^{∞}. As a result, the H-catalyzed propyne−allene isomerization channel, eq 4, is approximately as fast as the reaction to form $CH_3 + C_2H_2$, eq 2, and cannot be neglected in modeling calculations. The rate coefficient for this channel was first estimated by Kiefer et al.[48] to 4.2 × 10^{-11} cm^3 s^{-1} with no significant temperature dependence. Davis et al.,[16] in their RRKM analysis, obtained a value of 3.1 × 10^{-11} cm^3 s^{-1} at 1300 K and pressures near 1 bar, and from our calculations, under the same conditions, we obtain 2.9 × 10^{-11} cm^3 s^{-1}. Generally, the deviations between our values and the results from ref 16 do not exceed 10% in the temperature range 1200−1400 K. In ref 17, reaction 4 is not considered. There is, of course, also a direct isomerization channel, $pC_3H_4 + M \rightarrow aC_3H_4 + M$ (see, e.g., ref 48). Under our conditions, however, its rate is too low to effectively compete with reaction 4 (rate coefficients in the order 10^2 to 10^3 s^{-1}).[48,49]

The kinetic data deduced from our calculations were used to model the experimental H atom time profiles. The data are collected in Table 3 together with the Arrhenius parameters for the H-producing reaction sequence, eqs 6 and 7, where in our temperature range, reaction 6 is the rate-determining step.[47] We note that $k_{6+7} = k_6$ had to be increased by a factor of ∼3 as compared to ref 47 to match the initial slope of the hydrogen atom profiles. With these data, we were able to reproduce all of our H atom time profiles within the experimental uncertainty. A typical plot is shown in Figure 5.

It is also interesting to note that our calculated rate coefficients for reaction −2, $C_2H_2 + CH_3 \rightarrow CH_3CCH + H$, agree reasonably well with the corresponding experimental data. In a recent study, Kislitsyn et al.[45] used laser photolysis/photoionization mass spectrometry to determine k_{-2} in the temperature range from 750 to 1000 K at comparatively low pressures between 5 and 35 mbar. The temperature dependence of the rate coefficient is expressed in the form $k_{-2}(T) = (6.3 \pm 2.9) \times 10^{-13} \exp[-(5011 \pm 422)\ \text{K}/T]$ cm^3 s^{-1}, which gives a value of $k_{-2}(1000\ \text{K}) = (4.2 + 5.1/-2.7) \times 10^{-15}$ cm^3 s^{-1}. The low-pressure limit of k_{-2} can be estimated from $k_{-2}^0 \sim k_{-2b}^{\infty} k_{-2a}^{\infty}/k_{2b}^{\infty}$,[45] and with our data from Table 1, it follows $k_{-2}^0(1000\ \text{K}) = 3.6 \times 10^{-15}$ cm^3 s^{-1}. This is well within the error margin of the experimental result from ref 45. To compare the data at the upper end of our temperature range, we rely on a work of Hidaka et al.[50] These authors studied the pyrolysis of methane in a shock tube (T = 1400−2200 K, P = 2.3−3.7 bar) and derived a temperature dependence of the form $k_{-2}(T) = 1.03 \times 10^{-11} \exp(-8555\ \text{K}/T)$ cm^3 s^{-1} from complex modeling; this yields $k_2(1400\ \text{K}) = 2.3 \times 10^{-14}$ cm^3 s^{-1}. Using again the above approximation for the low-pressure limit, we obtain from our data $k_{-2}^0(1400\ \text{K}) = 4.1 \times 10^{-14}$ cm^3 s^{-1} in reasonable accord. We emphasize that this discussion is only to show the general consistency of our calculated data. It is not our intention to elucidate the $CH_3 + C_2H_2$ reaction in detail. For this, the reader is referred, for example, to ref 15, 16, and 45 and the literature cited therein.

5. Summary

The kinetics of the $pC_3H_4 + H$ reaction was experimentally studied over an extended temperature and pressure range. On the basis of the quantum chemical calculations and statistical rate theory, the temperature dependence as well as the missing pressure dependence of the rate coefficient was rationalized and found to be in accord with a complex-forming mechanism leading to $CH_3 + C_2H_2$. A parallel direct abstraction channel to give $C_3H_3 + H_2$ contributes to less than 10% under our conditions. Furthermore, a hydrogen atom catalyzed propyne−allene isomerization was shown to be important with a rate comparable to that of the $CH_3 + C_2H_2$ product channel. Thermochemical and kinetic parameters were computed, and readily applicable parametrizations of the rate coefficients for kinetic modeling were given. Our experimental and theoretical results are in line with the results of earlier theoretical works.

Acknowledgment. Financial support by the Deutsche Forschungsgemeinschaft (SFB 551 "Kohlenstoff aus der Gasphase: Elementarreaktionen, Strukturen, Werkstoffe") is gratefully acknowledged.

Supporting Information Available: Rate coefficients with detailed reaction conditions, and rotational constants and scaled harmonic wave numbers for all relevant molecules and transition states. This material is available free of charge via the Internet at http://pubs.acs.org.

References and Notes

(1) Miller, J. A.; Melius, C. F. *Combust. Flame* **1992**, *91*, 21.
(2) Homann, K.-H. *Angew. Chem., Int. Ed. Engl.* **1998**, *37*, 2434.

(3) Richter, H.; Howard, J. B. *Prog. Energy Combust. Sci.* **2000**, *26*, 565.
(4) Frenklach, M. *Phys. Chem. Chem. Phys.* **2002**, *4*, 2028.
(5) Miller, J. A.; Pilling, M. J.; Troe, J. *Proc. Combust. Inst.* **2005**, *30*, 43.
(6) McEnally, C. S.; Pfefferle, L. D.; Atakan, B.; Kohse-Höinghaus, K. *Prog. Energy Combust. Sci.* **2006**, *32*, 247.
(7) Brown, J. M.; Thrush, B. A. *Trans. Faraday Soc.* **1967**, *63*, 630.
(8) Wagner, H. Gg.; Zellner, R. *Ber. Bunsen-Ges. Phys. Chem.* **1972**, *76*, 518.
(9) Whytock, D. A.; Payne, W. A.; Stief, L. J. *J. Chem. Phys.* **1976**, *65*, 191.
(10) Hidaka, Y.; Nakamura, T.; Miyauchi, A.; Shiraishi, T.; Kawano, H. *Int. J. Chem. Kinet.* **1989**, *21*, 643.
(11) Warnatz, J.; Bockhorn, H; Möser, A.; Wenz, H. W. *Proc. Combust. Inst.* **1982**, *19*, 197.
(12) Wu, C. H.; Kern, R. D. *J. Chem. Phys.* **1987**, *91*, 6291.
(13) Ancia, R.; Vandooren, J.; Van Tiggelen, P. J. *Proc. Combust. Inst.* **1996**, *26*, 1009.
(14) Dean, A. M.; Westmoreland, P. R. *Int. J. Chem. Kinet.* **1987**, *19*, 207.
(15) Diau, E. W.; Lin, M. C.; Melius, C. F. *J. Chem. Phys.* **1994**, *101*, 3923.
(16) Davis, S. G.; Law, C. K.; Wang, H. *J. Phys. Chem. A* **1999**, *103*, 5889.
(17) Wang, B.; Hou, H.; Gu, Y. *J. Chem. Phys.* **2000**, *112*, 8458.
(18) Eng, R. A.; Fittschen, C.; Gebert, A.; Hibomvschi, P.; Hippler, H.; Unterreiner, A.-N. *Proc. Combust. Inst.* **1998**, *27*, 211.
(19) Fernandes, R. X.; Giri, B. R.; Hippler, H.; Kachiani, C.; Striebel, F. *J. Phys. Chem. A* **2005**, *109*, 1063.
(20) Gardiner, W. C., Jr.; Walker, B. F.; Wakefield, C. B. In *Shock Waves in Chemistry;* Lifshitz, A., Ed.; Marcel Dekker: New York, 1981, p 319.
(21) Apple, D.; Appleton, J. P. *Proc. Combust. Inst.* **1975**, *15*, 701.
(22) Just, Th. In *Shock Waves in Chemistry;* Lifshitz, A., Ed.; Marcel Dekker: New York, 1981, p 279.
(23) Frisch, M. J.; Trucks, G. W.; Schlegel, H. B.; Scuseria, G. E.; Robb, M. A.; Cheeseman, J. R.; Montgomery, J. A., Jr.; Vreven, T.; Kudin, K. N.; Burant, J. C.; Millam, J. M.; Iyengar, S. S.; Tomasi, J.; Barone, V.; Mennucci, B.; Cossi, M.; Scalmani, G.; Rega, N.; Petersson, G. A.; Nakatsuji, H.; Hada, M.; Ehara, M.; Toyota, K.; Fukuda, R.; Hasegawa, J.; Ishida, M.; Nakajima, T.; Honda, Y.; Kitao, O.; Nakai, H.; Klene, M.; Li, X.; Knox, J. E.; Hratchian, H. P.; Cross, J. B.; Bakken, V.; Adamo, C.; Jaramillo, J.; Gomperts, R.; Stratmann, R. E.; Yazyev, O.; Austin, A. J.; Cammi, R.; Pomelli, C.; Ochterski, J. W.; Ayala, P. Y.; Morokuma, K.; Voth, G. A.; Salvador, P.; Dannenberg, J. J.; Zakrzewski, V. G.; Dapprich, S.; Daniels, A. D.; Strain, M. C.; Farkas, O.; Malick, D. K.; Rabuck, A. D.; Raghavachari, K.; Foresman, J. B.; Ortiz, J. V.; Cui, Q.; Baboul, A. G.; Clifford, S.; Cioslowski, J.; Stefanov, B. B.; Liu, G.; Liashenko, A.; Piskorz, P.; Komaromi, I.; Martin, R. L.; Fox, D. J.; Keith, T.; Al-Laham, M. A.; Peng, C. Y.; Nanayakkara, A.; Challacombe, M.; Gill, P. M. W.; Johnson, B.; Chen, W.; Wong, M. W.; Gonzalez, C.; Pople, J. A. *Gaussian 03*, revision C.02; Gaussian, Inc.: Wallingford, CT, 2004.
(24) Parr, R. G.; Yang, W. *Density-functional theory of atoms and molecules;* Oxford University Press: Oxford, U.K., 1989.
(25) Becke, A. D. *J. Chem. Phys.* **1993**, *98*, 5648.
(26) Hehre, W. J.; Radom, L.; v.R. Schleyer, P.; Pople, J. A. *Ab Initio Molecular Orbital Theory;* Wiley: New York, 1986.
(27) Pople, J. A.; Head-Gordon, M.; Raghavachari, K. *J. Chem. Phys.* **1987**, *87*, 5968.
(28) Dunning, T. H., Jr. *J. Chem. Phys.* **1989**, *90*, 1007.
(29) Scott, A. P.; Radom, L. *J. Phys. Chem.* **1996**, *100*, 16502.
(30) Glasstone, S.; Laidler, K. J.; Eyring, H. *The Theory of Rate Processes;* McGraw-Hill: New York, 1941.
(31) Steinfeld, J. I.; Francisco, J. S.; Hase, W. L. *Chemical Kinetics and Dynamics;* Prentice Hall: Englewood Cliffs, NJ, 1989.
(32) Gilbert, R. G.; Smith, S. C. *Theory of Unimolecular and Recombination Reactions;* Blackwell: Oxford, U.K., 1990.
(33) Holbrook, K. A.; Pilling, M. J.; Robertson, S. H. *Unimolecular Reactions*, 2nd ed.; Wiley: Chichester, U.K., 1996.
(34) Forst, W. *Unimolecular Reactions;* Cambridge University Press: Cambridge, U.K., 2003.
(35) Schranz, H. W.; Nordholm, S. *Chem. Phys.* **1984**, *87*, 163.
(36) Snider, N. *J. Chem. Phys.* **1984**, *80*, 1885.
(37) Smith, S. C.; McEwan, M. J.; Gilbert, R. G. *J. Chem. Phys.* **1989**, *90*, 4265.
(38) Miller, J. A.; Klippenstein, S. J. *J. Phys. Chem. A* **2006**, *110*, 10528.
(39) Marcus, R. A.; Rice, O. K. *J. Phys. Colloid Chem.* **1951**, *55*, 894. Marcus, R. A. *J. Chem. Phys.* **1952**, *20*, 359.
(40) Troe, J. *J. Chem. Phys.* **1983**, *79*, 6017.
(41) Beyer, T.; Swinehart, D. F. *Commun. ACM* **1973**, *16*, 379.
(42) Astholz, D. C.; Troe, J.; Wieters, W. *J. Chem. Phys.* **1979**, *70*, 5107.
(43) Press, W. H.; Flannery, B. P.; Teukolski, S. A.; Vetterling, W. T. *Numerical Recipes in Fortran*, 2nd ed.; Cambridge University Press: Cambridge, U.K., 1992.
(44) Olzmann, M. *Phys. Chem. Chem. Phys.* **2002**, *4*, 3614.
(45) Kislitsyn, M. N.; Slagle, I. R.; Knyazev, V. D. *Proc. Combust. Inst.* **2002**, *29*, 1237.
(46) Kiefer, J. H.; Al-Alami, M. Z.; Budach, K. A. *J. Phys. Chem.* **1982**, *86*, 808.
(47) Kumaran, S.; Su, M.-C.; Lim, K. P.; Michael, J. V. *Proc. Combust. Inst.* **1996**, *26*, 605.
(48) Kiefer, J. H.; Mudipalli, P. S.; Sidhu, S. S., Kern, R. D.; Jursic, B. S.; Xie, K.; Chen, H. *J. Phys. Chem. A* **1997**, *101*, 4057.
(49) Miller, J. A.; Klippenstein, S. J. *J. Phys. Chem. A* **2003**, *107*, 2680.
(50) Hidaka, Y.; Nakamura, T.; Tanaka, H.; Inami, K.; Kawano, H. *Int. J. Chem. Kinet.* **1990**, *22*, 701.